Catalysis Science & Technology

ROYAL SOCIETY OF CHEMISTRY

PAPER

View Article Online
View Journal | View Issue

Cite this: *Catal. Sci. Technol.*, 2022, 12, 3727

Selective oxidation of methane to methanol and methyl hydroperoxide over palladium modified MoO_3 photocatalyst under ambient conditions†

Songmei Sun,*[abc] Nicholas F. Dummer,*[a] Takudzwa Bere,[a] Alexandra J. Barnes,[a] Greg Shaw,[a] Mark Douthwaite,[a] Samuel Pattisson,[a] Richard J. Lewis,[a] Nia Richards,[a] David J. Morgan[a] and Graham J. Hutchings*[a]

Received 2nd February 2022,
Accepted 1st May 2022

DOI: 10.1039/d2cy00240j

rsc.li/catalysis

Selective partial oxidation of methane to valuable oxygenated products remains a great challenge, as typically over oxidation of oxygenated products to CO_x is observed. Weak oxidative species on the catalyst surface have a great potential to overcome this limitation. However, weak oxidative species usually have low concentrations and are easily decomposed. Here we report a Pd/MoO_3 photocatalyst which can realize excellent methane oxidation to methanol and methyl hydroperoxide in pure water, under simulated solar light by *in situ* generated H_2O_2 at room temperature and pressure. The combined selectivity for methanol and methyl hydroperoxide is up to 98.6%, representing a productivity rate of 42.5 μmol g_{cat}^{-1} h^{-1}. Further studies on the reaction mechanism indicate that PdO species on the Pd loaded MoO_3 catalyst play an essential role in the suppression of over oxidation. In this case PdO traps the photo-generated electrons, leaving photo-generated holes for decomposition of H_2O_2 into weak oxidative hydroperoxyl radicals which are not involved in the formation of over oxidation products.

1. Introduction

Selective partial oxidation of methane has remained one of the major challenges in catalysis within the scientific community for over a century.[1–5] The primary obstacle of this reaction stems from the highly symmetrical tetrahedral structure of methane with the high bond energy of the C–H bond (440 kJ mol^{-1}).[6,7] Consequently, conditions that are sufficient to activate methane usually induce undesired over oxidation of oxygenated products (such as methanol and formaldehyde) to CO_x, since bond strengths in these oxygenated species are typically much lower (ΔH_{C-H} = 373.5 kJ mol^{-1} for methanol) than those of methane.

Due to the relative inertness of methane, the current industrial route for methane oxidation to partial oxidation products is indirect *via* the formation of synthesis gas (a mixture of CO and H_2) at high temperatures and pressures.[8,9] Such an approach, however, is energy-intensive and not economically feasible for more local, small-scale facilities.[10,11] Consequently, a number of different approaches for direct oxidation of methane to partial oxidation product have been proposed in recent years. For instance, homogeneous oxygenation of methane to alcohol esters, such as methyl bisulfate and methyl trifluoroacetate, can be achieved at impressive yields and selectivity by electrophilic metal catalysts (such as Hg, Pd, Pt, Au, Pb, Tl, Cu complexes),[12–17] but these systems are limited by the highly corrosive solvent and the lack of a fully closed catalytic cycle. Chemical looping systems exhibit high selectivity on methane oxidation to methanol over transition-metal exchanged zeolites with O_2, N_2O or H_2O as the oxidants.[18–20] However, high temperatures (200 to 500 °C) are required to activate the oxidant and desorb CH_3OH. Recently, Hutchings and co-workers reported an alternative approach for low-temperature selective oxidation of methane to methanol with H_2O_2 as an oxidant at 50 °C.[21–24] The typical Fe and Cu modified MFI-type zeolite catalyst have exhibited considerable activity for the oxidation of methane to methanol, achieving turnover frequencies (TOFs) of >2200 h^{-1} and methanol selectivities above 80%.[22] Likewise, methane oxidation using supported gold–palladium nanoparticles (NPs) or gold–palladium colloids under mild aqueous conditions with H_2O_2 as an oxidant were also reported through a radical mechanism.[21,23] Nevertheless, the

[a] *Max Planck-Cardiff Centre on the Fundamentals of Heterogeneous Catalysis FUNCAT, Cardiff Catalysis Institute, School of Chemistry, Cardiff University, Main Building, Park Place, Cardiff, CF10 3AT, UK. E-mail: sunsm@dhu.edu.cn, dummernf@cardiff.ac.uk, hutch@cardiff.ac.uk*
[b] *Donghua University, College of Environmental Science and Engineering, Shanghai 201620, P.R. China*
[c] *Shanghai Institute of Pollution Control and Ecological Security, Shanghai 200092, P.R. China*

† Electronic supplementary information (ESI) available. See DOI: https://doi.org/10.1039/d2cy00240j

relatively high cost of H_2O_2 for even stoichiometric oxidation of CH_4 as well as the high pressure (30 bar) used in this reaction makes it difficult to envisage an economically viable process based on this chemistry.

Direct methane oxidation by photocatalysis is emerging as a promising green strategy, which utilizes photons instead of high temperatures and pressures to drive this reaction at ambient conditions. Despite this, there are few reports of photocatalytic processes for methane oxidation with satisfactory selectivity and productivity.[25–30] The selectivity to the primary products (CH_3OH and CH_3OOH) is typically reported to be lower than 50%, with a productivity rate in pure water of no more than 20 μmol g_{cat}^{-1} h^{-1}.[25–28] Accordingly, the process of methane activation can be considered the central issue in photocatalytic methane oxidation. Among the reported articles, the most prevalent way to activate methane in photocatalysis is *via* photogenerated holes or $^{\bullet}OH$ radicals to generate $^{\bullet}CH_3$ radicals. However, the oxidation ability of photogenerated holes are stronger than $^{\bullet}OH$ radicals in most of the oxide semiconductor photocatalysts, because of their low valence band positions. Furthermore, it has been reported that excess $^{\bullet}OH$ radicals also result in over oxidation of CH_3OH to HCOOH and CO_2.[22,31] Based on these reasons, CO_2 is usually reported as the primary product from direct methane oxidation by photocatalysis.[25–28]

Herein, we report palladium supported on molybdenum trioxide nanobelts (Pd/MoO_3) as an efficient photocatalyst for methane oxidation to methanol in water. The reaction proceeds at room temperature and atmospheric pressure under simulated solar light irradiation, by using water as the initial oxidant source. The combined selectivity to CH_3OOH and CH_3OH from direct methane oxidation was found to be over 97%. Further study indicates that the direct methane oxidation is realized by *in situ* generated peroxy species from water oxidation on the catalyst surface. We consider that this work advances the opportunity to use methane as a C_1 starting material together with water and sunlight to make an important and in-demand chemical intermediate.

2. Experimental section

2.1. Photocatalyst preparation

All the chemicals involved were of analytical grade and used without further purification. For the pure MoO_3 sample, 1 mmol $(NH_4)_6Mo_7O_{24}{\cdot}4H_2O$ dispersed in 50 mL deionized water. After vigorous stirring for 1 h, the pH value was adjusted to 1 by addition of 4 M HNO_3. After stirring for 5 h, the volume of the precursor suspension was adjusted to 80 mL by adding additional deionized water, and then the suspension was transferred to a 100 mL Teflon-lined autoclave. The sealed reaction system was heated at 180 °C for 18 h. The system was then allowed to cool down to room temperature. The obtained solid products were collected by centrifugation, washed with 600 mL deionized water for three times, and then dried at 50 °C overnight for further characterization. Three Pd/MoO_3 samples were prepared with different Pd loadings. Typically, 0.1 g pure MoO_3 sample dispersed in 100 mL deionized water and 5 mL 2-propanol. A certain amount of $PdCl_2$ solution (*e.g.* 10 mg mL^{-1}) was added in the above MoO_3 suspension by vigorous stirring under 300 W xenon light irradiation at 25 °C. After 12 h, the suspension was centrifuged, washed, dried at 50 °C overnight and then heated at 300 °C under N_2 flow for 1 h. The Pd loading amount was calculated from inductively coupled plasma optical emission spectrometry (ICP-OES) and was 0.92, 1.86 and 3.75 wt%.

2.2. Characterization

The purity and the crystallinity of the as-prepared samples were characterized by powder X-ray diffraction (XRD) on a PANalytical X'Pert Pro X-ray diffractometer using Cu $K\alpha_1$ radiation (λ = 0.154098 nm) while the voltage and electric current were held at 40 kV and 40 mA. The transmission electron microscope (TEM) analyses were performed by a Hitachi HF5000 spherical aberration corrected transmission electron microscope. X-ray photoelectron spectroscopy (XPS) was performed using a Kratos Axis Ultra DLD spectrometer. Samples were mounted using double-sided adhesive tape and binding energies were referenced to the C 1s binding energy of adventitious carbon contamination, which taken to be 284.8 eV. Monochromatic AlKα radiation was used for all measurements; an analyser pass energy of 160 eV was used for survey scans while 40 eV was employed for detailed regional scans. Quantification was performed using CasaXPS v2.3.32 (ref. 32) after subtraction of a Shirley background and using modified Wagner elemental sensitivity factors as supplied by the instrument manufacturer. UV-vis spectrophotometer diffuse reflectance spectrum (DRS) of the sample was measured using an Agilent Cary 60 UV-vis spectrophotometer. The *in situ* DRIFT measurement was performed on a Bruker Tensor 27 spectrometer fitted with a HgCdTe (MCT) detector and a Harrick Praying Mantis HVC-DRP-4 cell equipped with KBr windows. ^{1}H NMR spectra were acquired on a Bruker 500 MHz Ultrashield NMR spectrometer. Superoxide and hydroxyl radical in the reaction system were analyzed by ESR spectrometry coupled to spin trapping with 5,5-dimethyl-1-pyrroline *N*-oxide (DMPO). In a typical experimental process, 5 mg of photocatalyst samples were dispersed in 1 mL deionized water by ultrasonic dispersion for about 1 min. 50 μL DMPO was added in the suspension. The reaction mixture was then transferred to a closed reaction cell, purged with N_2 for 10 min and exposed to simulated light irradiation for 10 min. After that, 50 μL aliquots of the sample solution was extracted and immediately transferred to a quartz capillary tube for an ESR spectrometer (Bruker EMX-8/2.7). Inductively coupled plasma optical emission spectrometry (ICP-OES) analyses were performed by Leeman Labs Prodigy7.

2.3. Photocatalytic test

Photocatalytic methane oxidation experiments were performed under a 300 W xenon light (Research Grade Xe Arc Lamp, Sciencetech) located approximately 10 cm from the sample. The light intensity was controlled at 150 mW cm^{-2}. The reaction cell (capacity 600 mL) was made of Pyrex glass with a quartz window on top. Typically, 0.01 g of the as-prepared photocatalyst powder was dispersed in 100 mL deionized water under sonication. Before illumination, pure CH_4 gas was slowly bubbled through the reaction vessel for 30 min to exhaust air. Then the reaction vessel was sealed and irradiated under the xenon light. During the photocatalytic tests, the temperature of the reaction vessel was maintained at 15 °C by providing a flow of cooling water through an external jacket. The concentration of the gas products was determined by gas chromatography (GC). The GC was equipped with a CP SIL5CB column (50 m, 0.33 mm internal diameter) fitted with a methanizer and analyzed by a flame ionization detector (FID). ^{1}H NMR was selected as the technique for analysis of the liquid phase product using D_2O as the solvent. All ^{1}H NMR samples were analyzed against a calibrated insert containing tetramethylsilane (TMS) in deuterated chloroform (99.9% D). The *in situ* generated H_2O_2 was determined by the titanium sulfate spectrophotometric method.

2.4. Electrochemical measurements

Electrochemical measurements were performed on a CHI 700E electrochemical workstation using a standard three-electrode cell with a working electrode, a platinum mesh as counter electrode, and a standard saturated calomel electrode (SCE) in saturated KCl as reference electrode. The working electrodes were prepared by dip-coating: Briefly, 5 mg of photocatalyst was suspended in 0.1 mL of ethanol in the presence of 1% Nafion to produce a slurry, which was then dipcoated onto a 2 cm × 1.5 cm FTO glass electrode and dried at 25 °C.

3. Results and discussion

3.1. Synthesis and structural characterization of MoO_3 and Pd/MoO_3

MoO_3 was chosen as the catalyst due to its narrow band gap (2.8 eV) and the appropriate band energy as potential catalyst for methane oxidation.[33] MoO_3 was prepared *via* a simple hydrothermal synthesis with HNO_3. Pd/MoO_3 sample was prepared by *in situ* photocatalytic reduction of $PdCl_2$ which was deposited onto the MoO_3 surface. The crystal structure of

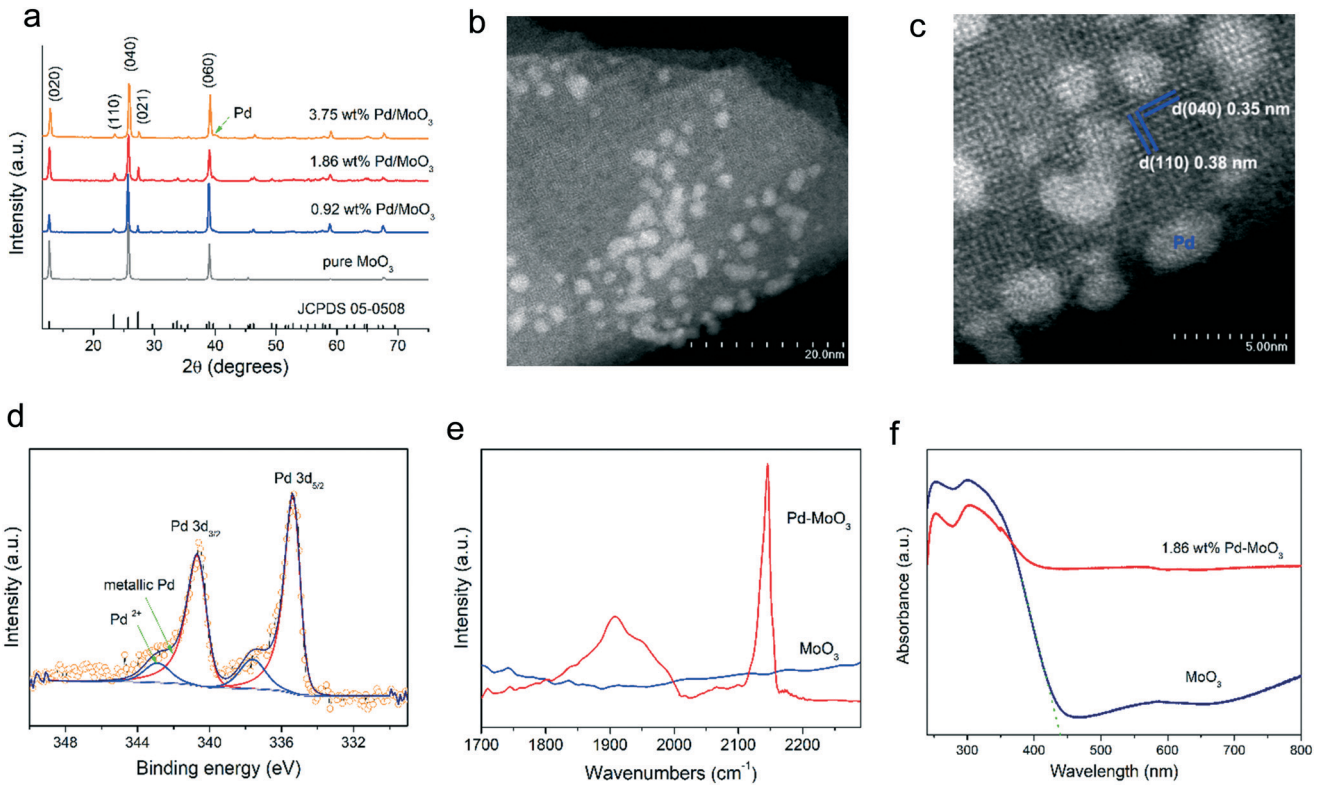

Fig. 1 Characterization of the parent MoO_3 and Pd/MoO_3 samples. (a) The XRD patterns for as-prepared MoO_3 and Pd/MoO_3 samples. (b) High-angle annular dark-field scanning transmission electron microscope (HAADF-STEM) image of 1.86 wt% Pd/MoO_3 sample. (c) High resolution STEM image of the 1.86 wt% Pd/MoO_3 sample detected from the edge of MoO_3 nanobelt in Fig. 1b. (d) Pd 3d XPS spectrum of the 1.86 wt% Pd/MoO_3 sample. (e) *In situ* DRIFTS of CO adsorption on MoO_3 and the 1.86 wt% Pd/MoO_3 sample. (f) Ultraviolet-visible absorption spectrum of the MoO_3 and the 1.86 wt% Pd/MoO_3 samples.

the as-prepared samples was firstly characterized by powder X-ray diffraction (XRD). Comparable diffraction patterns were recorded for both the MoO_3 and Pd/MoO_3 samples (Fig. 1a). All diffraction peaks were indexed to the orthorhombic phase of MoO_3 [space group *Pbnm*, (JCPDS) No. 05-0508]. However, the relative diffraction intensity of (040) peak over the (110) and (021) peak in MoO_3 was much greater than the standard values from JCPDS 05-0508, indicating that the MoO_3 samples in this study may have grown anisotropically along the [010] direction. The characteristic diffraction peak of metallic Pd is observed in the 1.86 and 3.75 wt% Pd/MO_3 samples. No characteristic diffraction peaks of Pd were observed by XRD with the 0.92 wt% Pd/MoO_3 sample, which may be ascribed to the low concentration and high dispersion of Pd on the MoO_3 surface.

The micro-structure of MoO_3 and Pd/MoO_3 were further investigated by transmission electron microscopy (TEM), as shown in Fig. S1a–f.† The MoO_3 particles exhibit an ultrathin nanobelt morphology (Fig. S1a–f†). Under scanning TEM (STEM), Pd clusters with a diameter of ≤4 nm were observed on the MoO_3 nanobelt (Fig. 1b). High resolution STEM images of the 1.86 wt% Pd/MoO_3 catalyst (Fig. 1c) confirmed that the main exposed surface of MoO_3 nanobelt is the (001) plane of the orthorhombic phase of MoO_3. When we increased the Pd loading amount to 3.75 wt%, much larger Pd particles (*ca.* 20 nm) were formed on the MoO_3 surface (Fig. S1f†), indicating that the 1.86 wt% is close to the optimal concentration for forming highly dispersed Pd species on MoO_3. The chemical states of the Pd species on the 1.86 wt% Pd/MoO_3 catalyst were characterized by X-ray photoelectron spectroscopy (XPS). As shown in Fig. 1d, the Pd 3d signal was fitted to two pairs of doublets. The main peaks centered at 335.4 and 340.7 eV are attributed to the $3d_{5/2}$ and $3d_{3/2}$ binding energies of metallic Pd^0, respectively.[34] The second doublet, with higher binding energies at 337.6 eV and 342.9 eV, are the signals from Pd^{2+}-species,[35] which can be rationalized by a PdO shell formed on the surface of Pd^0 species. The atomic ratio of Pd^0/Pd^{2+} was calculated to be *ca.* 5. The XPS spectra of O 1s and Mo 3d recorded on the 1.86 wt% Pd/MoO_3 sample are illustrated in Fig. S2,† and are comparable to the reported data for Pd deposited on oxygen deficient MoO_3.[36] To further identify the Pd species on the catalyst surface, *in situ* diffuse reflection infrared Fourier transform spectroscopy (DRIFTS) of adsorbed carbon monoxide, a common probe molecule,[37] was used. Before each measurement, the sample was preheated under vacuum at 298 K for 1 hour. After saturation with CO, the sample was evacuated by an N_2 purge under room temperature for 1 h and then the DRIFT spectrum of adsorbed CO on the sample was acquired. No CO absorption was observed on the pure MoO_3 sample, while two absorption bands were observed for the Pd/MoO_3 catalyst. As shown in Fig. 1e, the sharp absorption peak at 2145 cm^{-1} on Pd/MoO_3 sample is related to strongly adsorbed, atop linear CO on the surface Pd oxide.[38] The broad absorption band around 1949 and 1907 cm^{-1} can be assigned to CO adsorbed at bridge and hollow sites of metallic Pd, respectively.[39] The results suggest that a portion of the surface PdO_x may have been reduced to metallic Pd by CO at ambient conditions. The optical absorption properties of the MoO_3 and Pd/MoO_3 samples were characterized by UV-vis diffuse reflectance spectra (DRS), as shown in Fig. 1f. The MoO_3 nanobelts can absorb light from the UV range up to about 440 nm in the visible range due to the intrinsic bandgap transition. According to the absorption spectrum, the band gap energy (E_g) of the MoO_3 nanobelts was estimated to be 2.8 eV. An increased light absorption beyond 440 nm is observed in the Pd/MoO_3 sample, implying that a higher concentration of excited electrons in the Pd/MoO_3 sample are present under simulated solar light irradiation.

3.2. Experimental evaluation on methane oxidation activities

Photocatalytic methane oxidation was performed in pure water and illuminated by a 300 W xenon lamp. It was found that the main products of methane oxidation over the Pd/MoO_3 samples were CH_3OH and CH_3OOH under full arc irradiation (Fig. 2a). There was no organic product in the reaction solution under non-illuminated conditions over the MoO_3 catalyst. Under light irradiation, the amount of CH_3OH increased almost linearly with irradiation time within 24 h and reached a final concentration of 55 μmol L^{-1} over 1.86 wt% Pd/MoO_3, corresponding to a methanol productivity of 22.9 μmol g_{cat}^{-1} h^{-1}. The concentration of CH_3OOH reached a highest value of 12 μmol L^{-1} at 8 h. After that, the amount of CH_3OOH decreased, indicating that the CH_3OOH may be the intermediate species for methanol production. During the methane oxidation process, only a small amount of CO_2 (0.15 μmol) was detected in the gas phase. The selectivity to primary products (CH_3OH and CH_3OOH) from 1.86 wt% Pd/MoO_3 was found to be 97.6% over 24 h irradiation. Without Pd loading, the primary product from methane oxidation over the parent MoO_3 support was HCOOH during 8 h of irradiation, with a selectivity of 50.5% (Fig. S3a†), CH_3OH only accounts for 27% over MoO_3 (Fig. S3a†).

To investigate the nature of the oxidative species, a series of experiments were conducted. The reaction proceeds under an atmosphere of methane with no additional gaseous oxidant, therefore, upon analysis of the reaction solution, H_2O_2 was detected in the reaction solution by means of titanium sulfate spectrophotometric method. The concentration of the *in situ* generated H_2O_2 reached 38 μmol L^{-1} after 8 h irradiation and this value was maintained at around 35–39 μmol L^{-1} during the following 16 h, over 1.86 wt% Pd/MoO_3 (Fig. 2b). Furthermore, the evolution of H_2O_2 along with irradiation time is very similar to that of CH_3OOH. We consider that *in situ* generated H_2O_2 may be the oxidative species for methane oxidation over Pd/MoO_3 to facilitate production of CH_3OOH. This inference is supported by following the H_2O_2 production under light irradiation as well as the photocatalytic performance over pure MoO_3, 0.92 wt% Pd/MoO_3 and 3.75 wt% Pd/MoO_3 (Fig. S3b–d†). As shown in

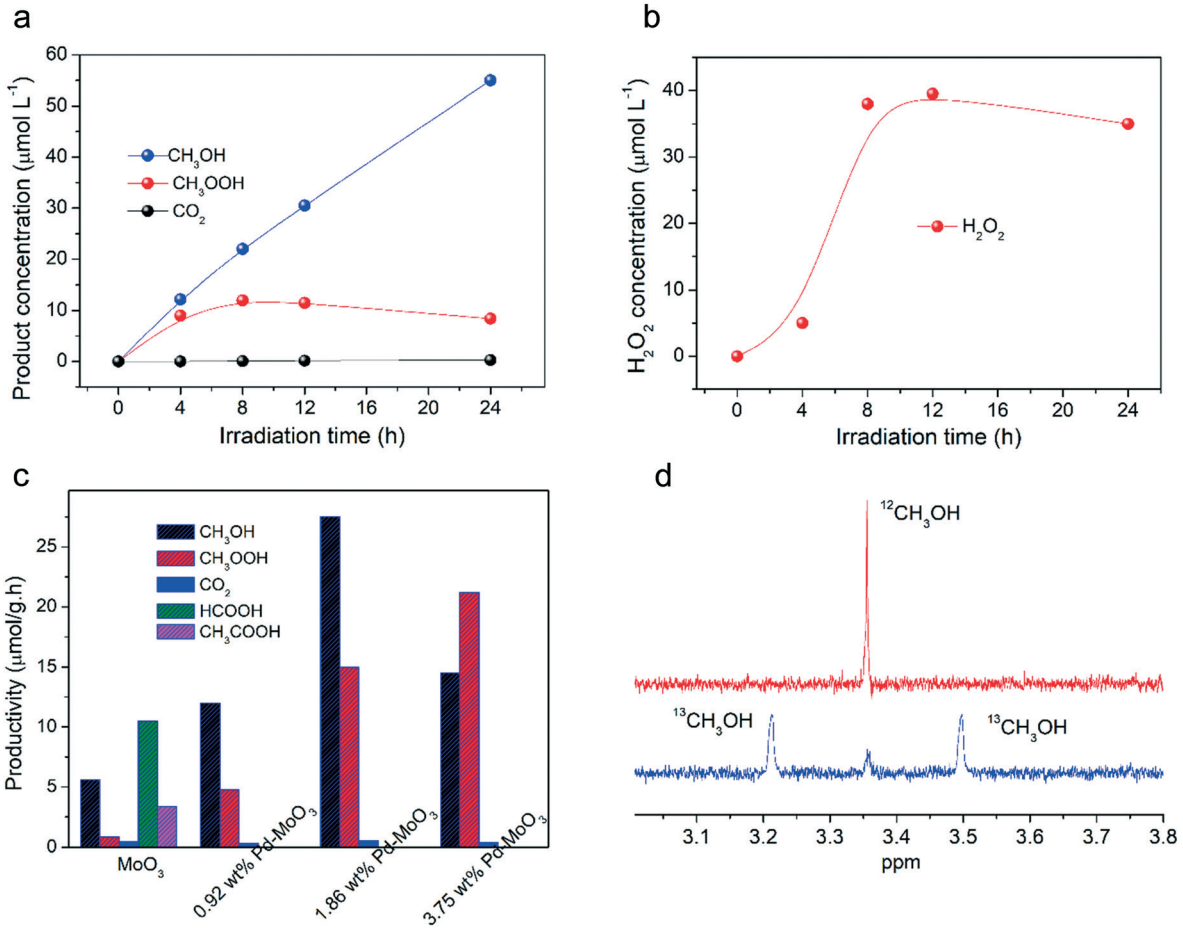

Fig. 2 Photocatalytic methane conversion over Pd/MoO_3 catalysts. (a) Methanol and methyl hydroperoxide yield as a function of irradiation time over 1.86 wt% Pd/MoO_3. (b) H_2O_2 yield as a function of irradiation time over 1.86 wt% Pd/MoO_3. (c) Comparison of photocatalytic methane oxidation performances of different Pd/MoO_3 samples at 8 h irradiation. (d) ^1H NMR spectra of the methanol product in D_2O-saturated water solution from $^{12}CH_4$ and $^{13}CH_4$ oxidation over 1.86 wt% Pd/MoO_3, respectively.

Fig. 2 and S3,† the H_2O_2 concentration increased rapidly under light irradiation after 4 h. The CH_3OOH productivity rate over 0.92 wt%, 1.86 wt% and 3.75 wt% Pd/MoO_3 was 4.5, 22.5, 26.0 μmol g_{cat}^{-1} h^{-1}, respectively, within 4 h. This productivity was maintained at 4.8, 15.0 and 21.2 μmol g_{cat}^{-1} h^{-1} over 8 h, following this the H_2O_2 production reached a plateau. Under these conditions, the CH_3OOH productivity over the Pd/MoO_3 catalysts decreased to 2.9, 3.5 and 8.9 μmol g_{cat}^{-1} h^{-1}, respectively. Although loading with Pd can increase the photocatalytic performance of MoO_3, it was found that excess Pd (3.75 wt%) decreased the generated H_2O_2 concentration and reduced the methane oxidation performance (Fig. S3b and d†). There are two possible reasons for this observation. First, although Pd is an active catalyst for H_2O_2 synthesis it is also a catalyst for its decomposition and this could be operating more effectively at higher Pd concentrations. Secondly, the Pd could block surface sites for the photo-oxidation reaction.

In our experiments, the optimum Pd loading amount was found to be 1.86 wt%, exhibited the highest respective CH_3OH and CH_3OOH productivity of 27.5 and 15 μmol g_{cat}^{-1} h^{-1} within 8 h (Fig. 2c), with a combined selectivity of 98.6% to CH_3OH and CH_3OOH.

To evaluate the stability of the Pd/MoO_3 catalyst, the used catalyst (1.86 wt% Pd/MoO_3) was centrifuged and dispersed in another 100 mL water to test the recyclability of the catalyst. As demonstrated in Fig. S4,† after three consecutive runs (72 h), the photocatalytic activity of the Pd/MoO_3 for methanol production gradually decreased from the first to the third cycle. The CH_3OH productivity rate over 1.86 wt% Pd/MoO_3 was 22.9, 21.3, 19.2 μmol g_{cat}^{-1} h^{-1}, respectively, from the first to the third cycle within each 24 h. The decreased activity may be ascribed to the leaching of Pd and the formation of H_xMoO_3 species on the catalyst surface. The concentration of Pd in the reaction solution from 1.86 wt% Pd/MoO_3 sample after 24 h irradiation is 148.24 μg L^{-1}, accounting for 7.9% of the loaded Pd amount from the 1.86 wt% Pd/MoO_3 sample. The XRD pattern (Fig. S5†) of the used Pd/MoO_3 sample confirmed the formation of H_xMoO_3 species after 72 h over the three photocatalytic reaction cycles. The formation of H_xMoO_3 is ascribed to hydrogen insertion in MoO_3 during photocatalytic methane

oxidation in water, donated *via* the hydrogen spillover phenomenon. Hydrogen spillover phenomenon is well-documented on WO_3 and MoO_3 photocatalysts.[40–42] After the formation of H_xMoO_3, the color of the Pd/MoO_3 catalyst was transformed from light gray to dark blue. These surface H_xMoO_3 species can be returned to MoO_3 following heat treatment in air.

To confirm that methanol was formed from a methane oxidation process, a series of control experiments over 1.86 wt% Pd/MoO_3 were carried out. There were no organic species found in the reaction solution before and after light irradiation when N_2 was used in place of methane. The photolysis experiment of methane in water under light irradiation indicates only trace amounts of methanol (4.2 μmol L^{-1}) were produced in the reaction solution after 24 h irradiation without a catalyst. The methanol concentration from methane photolysis increased to 11.5 μmol L^{-1} where a 50 μmol L^{-1} H_2O_2 solution was used after 24 h irradiation. However, this concentration is still much lower than the value of 55 μmol L^{-1} formed over Pd/MoO_3 under the same conditions, indicating that Pd/MoO_3 performed as a catalyst for this reaction.

Experiments using isotopically labelled components were carried out over Pd/MoO_3 for the selective methane oxidation to methanol. The corresponding ^1H NMR spectrum for the products obtained from $^{13}CH_4$ and $^{12}CH_4$ oxidation is given in Fig. 2d. Where $^{12}CH_4$ was used as the initial reactant, only a singlet was observed around 3.35 ppm, which is the characteristic methyl proton peak for $^{12}CH_3OH$ in D_2O. However, with the isotopically labelled $^{13}CH_4$, the methyl proton resonance was observed as a doublet at 3.2 and 3.5 ppm, which is the characteristic methyl proton peak for $^{13}CH_3OH$ in D_2O. These studies clearly show that the CH_3OH product indeed comes from methane oxidation.

3.3. *In situ* DRIFT studies

From our observations that the Pd/MoO_3 samples exhibit high selectivity to methanol from methane oxidation, we sought to rationalize why CO_2 was not the main product, as

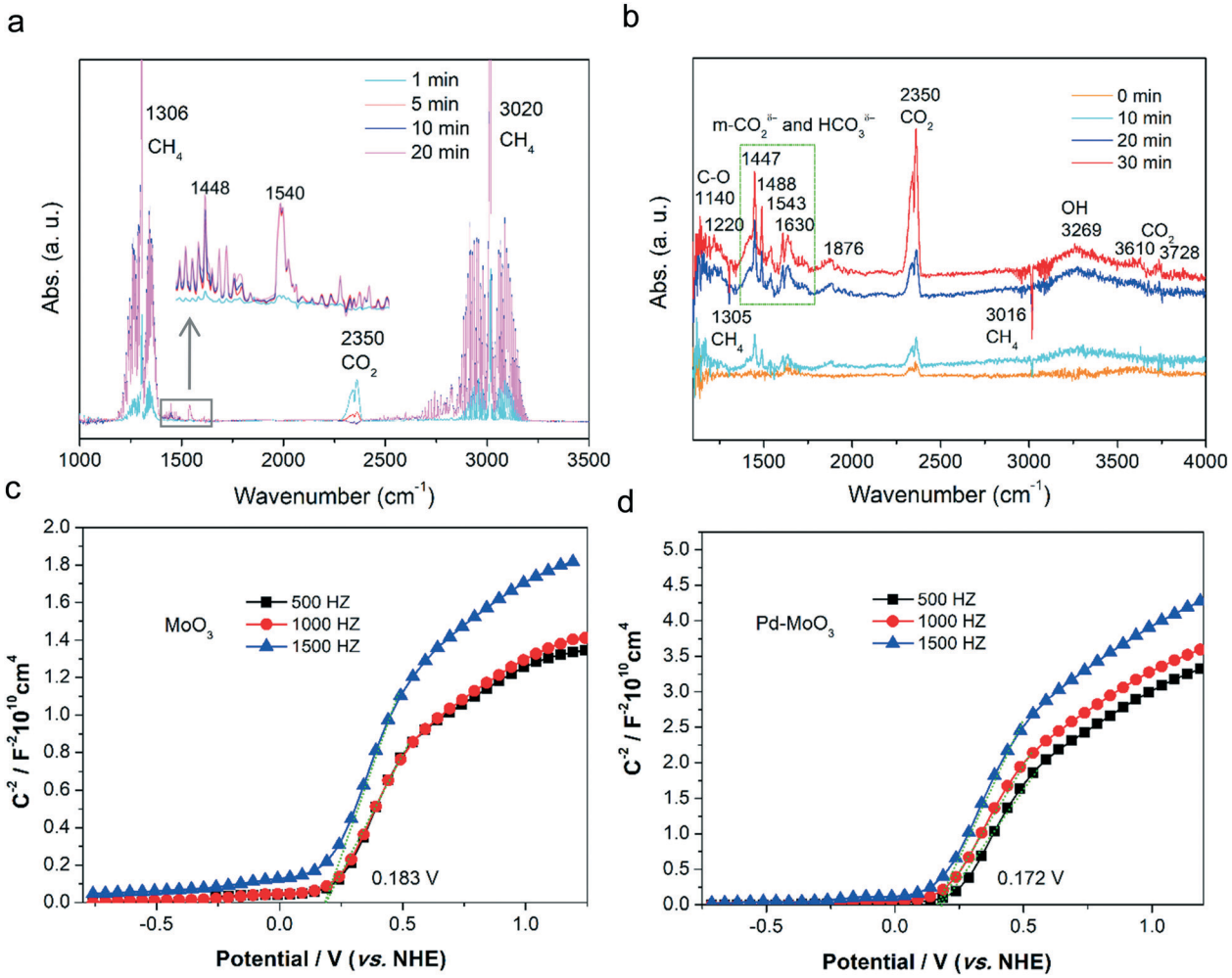

Fig. 3 Methane adsorption and electrochemical characterizations. (a) *In situ* DRIFT spectra of methane adsorption on the 1.86 wt% Pd/MoO_3 catalyst under dark. (b) *In situ* DRIFT spectra of methane oxidation on the 1.86 wt% Pd/MoO_3 catalyst under light irradiation. Mott–Schottky plot of the as-prepared MoO_3 (c) and 1.86 wt% Pd/MoO_3 (d) electrode in 0.1 M Na_2SO_4.

reported over other photocatalysts.[25–28] A DRIFTs study was performed on the catalysts to understand the adsorption and activation mechanism of methane. Prior to introducing methane, the catalyst was pretreated by N_2 purging in a vacuum chamber for 1 h at room temperature. After the pretreatment, the background DRIFT spectrum of the MoO_3 and Pd/MoO_3 catalysts was recorded. The surface of both MoO_3 and Pd/MoO_3 were dominated by strongly adsorbed OH and CO_2 in the vacuum state (Fig. S6a and b†). The most intense absorption bands on 1.86 wt% Pd/MoO_3 are seen at 1457, 1556, 1655, 2350, 3236 and 3350 cm^{-1}. These bands are characteristic vibration modes of adsorbed bicarbonate $HCO_3^{\delta-}$ (1457, 1655), monodentate $CO_2^{\delta-}$ (1556), linear CO_2 (2350) and surface OH (3236, 3350 cm^{-1}).[43–45] *In situ* DRIFT spectra of methane adsorption on the catalysts were then recorded. As shown in Fig. 3a, the absorption band at 1306 and 3020 cm^{-1} originate from the physisorption of CH_4, achieving saturation after 10 min. It is interesting that the absorption band from linear CO_2 decreased along with the increase of CH_4 absorption. Before investigating the adsorption of CH_4, the catalyst was pretreated by nitrogen purging under evacuation conditions. We can confirm that the adsorption of linear CO_2 could not have been further decreased by gas purging. Therefore, the further decreased absorption from linear CO_2 after introducing methane is ascribed to the overlap of CH_4 on pre-adsorbed CO_2. Besides the linear CO_2 sites, CH_4 also adsorbed on the bicarbonate $HCO_3^{\delta-}$ (1457) and monodentate CO_2^{δ} (1556) sites, resulting in the red-shift of the bicarbonate $HCO_3^{\delta-}$ and monodentate CO_2^{δ} absorption band to 1448 and 1540 cm^{-1}, respectively (Fig. 3a). All of these DRIFT features indicate that the active sites for CO_2 and CH_4 adsorption and activation may be the same on the Pd/MoO_3 catalyst.

Under light irradiation, it was found that absorption from physisorbed CH_4 rapidly decreased along with the largely increased absorption from carbonate species (1447–1630 cm^{-1}) and linear CO_2 (2350 cm^{-1}) (Fig. 3b). These changes recorded on the DRIFT spectrum are ascribed to the increased exposure of CO_2 after CH_4 escaped from the surface under light irradiation, further indicating the CH_4 and CO_2 molecules may be adsorbed on the same reactive sites. In addition to these existing absorption bands from carbonate species, linear CO_2 and physisorbed CH_4, there are two new absorption bands which appear under light irradiation. The new formed absorption band at approximately 1140 cm^{-1} is likely the C–O stretching band of the C–OH from methane oxidation. Another broad absorption *ca.* 3269 cm^{-1} is from the surface O–H group. The increase of O–H absorption band is ascribed to the proton transfer from water to MoO_3 catalyst surface during the formation of H_2O_2 and methane oxidation process, which will be discussed in detail in the following section.

3.4. Electrochemical performance of MoO_3 and Pd/MoO_3

Generally, there are two ways that H_2O_2 can be generated photocatalytically; *via* O_2 reduction or water oxidation. In this experiment, there is no oxygen in the reaction cell, therefore, it is most likely that the H_2O_2 is generated from water oxidation. To investigate the thermodynamic feasibility of the MoO_3 and Pd/MoO_3 samples for *in situ* water oxidation to produce H_2O_2, the conduction and valence band potentials of the catalysts were studied by electrochemical measurements. Fig. 3c and d show the electrochemical Mott–Schottky plot of pure MoO_3 and 1.86 wt% Pd/MoO_3 samples on a fluorine-doped tin oxide (FTO) substrate, from which respective flat band potentials (E_{fb}) were calculated to be 0.183 and 0.172 V *versus* normal hydrogen electrode (NHE) at pH 7. As an n-type semiconductor, the conduction band potential of MoO_3 (E_{cb}) is considered to be *ca.* 0.1 V above the E_{fb}. Then, respective E_{cb} values of the MoO_3 and Pd/MoO_3 samples were estimated at 0.083 and 0.072 V *versus* NHE at pH 7. The band gap energy (E_g) of MoO_3 and Pd/MoO_3 calculated from UV-vis diffuse reflectance spectra was 2.8 eV. Therefore, the valence band potentials (E_{vb}) of MoO_3 and Pd/MoO_3 can be calculated at 2.717 and 2.728 V *versus* NHE at pH 7, respectively. The redox potential for H_2O_2 generation *via* two-electron oxidation of water is 1.36 V *versus* NHE at pH 7. From the thermodynamic point of view, it is probable that H_2O_2 may be generated over MoO_3 and Pd/MoO_3 photocatalytically from water oxidation, considering that there is no O_2 in the reaction cell to generate H_2O_2 and furthermore the dramatically increased CO_2 production if a small amount of O_2 (0.5% volume) was introduced in the CH_4 oxidation reaction cell.

To study why the Pd/MoO_3 sample exhibited higher activity for H_2O_2 production, we measured the current–voltage (J–V) curves for the MoO_3 and Pd/MoO_3 samples under light illumination. As shown in Fig. S7,† the over potential at 0.5 mA cm^{-2} for the Pd/MoO_3 electrode is 22 mV lower than that of MoO_3, suggesting a decreased kinetic barrier for water oxidation on the Pd/MoO_3 surface. The smaller Tafel slope (221 mV dec^{-1}, Fig. S7 inset†) from the Pd/MoO_3 sample further revealed the improved water oxidation performance.

3.5. Photocatalytic mechanism

To study the photocatalytic methane oxidation mechanism further, electron spin resonance (ESR) was performed with the spin trap 5,5-dimethyl-1-pyrroline *N*-oxide (DMPO) to determine the oxidative species formed over the simulated sunlight irradiated MoO_3 and Pd–MoO_3 photocatalysts. As shown in Fig. 4a, both characteristic peaks of DMPO–HO$^{\bullet}$ and DMPO–HOO$^{\bullet}$ species are observed over pure MoO_3 and 1.86 wt% Pd–MoO_3 samples under simulated sunlight irradiation in water, while no ESR signal can be detected in the dark over 1.86 wt% Pd–MoO_3, which indicates that $^{\bullet}$OH and $^{\bullet}$OOH radicals are indeed generated on the surface of the photocatalyst after irradiation. Besides, it was found the intensities of the DMPO–HOO$^{\bullet}$ and DMPO–HO$^{\bullet}$ signals formed over Pd–MoO_3 sample are obviously higher than those over the pure MoO_3 sample, suggesting that the

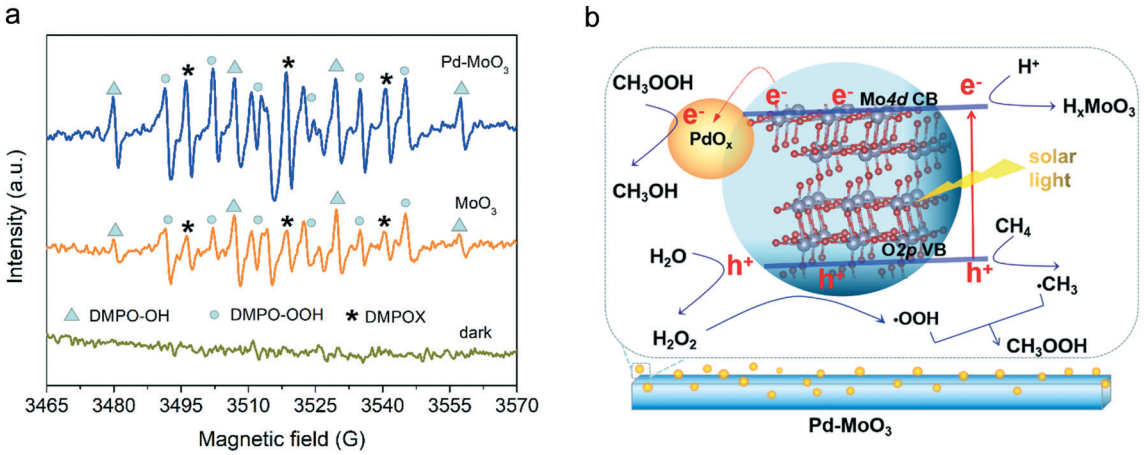

Fig. 4 Mechanistic study for the photocatalytic methane oxidation over MoO_3 and Pd–MoO_3. (a) DMPO spin-trapping ESR spectra for DMPO–HO˙ (signals marked with triangle) and DMPO–HOO˙ (signals marked with circle) in aqueous suspensions of MoO_3 and 1.86 wt% Pd–MoO_3 samples, signals marked by asterisks belong to the existing oxidation product of DMPO, 5,5-dimethyl-2-oxopyrroline-1-oxyl (DMPOX). (b) The proposed mechanism for photocatalytic H_2O_2 generation and methane oxidation conversion over Pd/MoO_3.

concentration of ˙OOH and ˙OH radicals formed on the surface of the Pd–MoO_3 photocatalyst are much higher than that on pure MoO_3. Furthermore, it is worth noting that the relative concentration of ˙OOH radicals was much higher than that of ˙OH radicals with the Pd–MoO_3 sample, while ˙OH radicals are predominant with MoO_3.

Based on the results and discussion above, we propose a reaction mechanism for selective methane oxidation to methanol (Fig. 4b). Under light irradiation, incident photons excite electrons from the valence band (oxygen 2p orbits) of MoO_3 to the conduction band (molybdenum 4d orbits), leaving holes on the oxygen atoms of MoO_3 (eqn (1)). In the Pd/MoO_3 sample, the photo-generated electrons in the conduction band of MoO_3 will transfer to the surface of Pd clusters (PdO) due to the higher work function of MoO_3 (−6.8 eV) than that of PdO (−7.9 eV).[46,47]

$$MoO_3 \xrightarrow{h\nu} MoO_3(h^+) + MoO_3(e^-) \quad (1)$$

$$2MoO_3(h^+) + 2H_2O \rightarrow H_2O_2 + 2H^+ \quad (2)$$

$$H_2O_2 + MoO_3(h^+) \xrightarrow{h\nu} {}^{\cdot}OOH + H^+ \quad (3)$$

$$CH_4 + MoO_3(h^+) \xrightarrow{h\nu} {}^{\cdot}CH_3 + H^+ \quad (4)$$

$${}^{\cdot}CH_3 + {}^{\cdot}OOH \rightarrow CH_3OOH \quad (5)$$

$$CH_3OOH + 2MoO_3(e^-) + 2H^+ \xrightarrow{h\nu} CH_3OH + H_2O \quad (6)$$

$$H_2O_2 + H^+ + MoO_3(e^-) \xrightarrow{h\nu} {}^{\cdot}OH + H_2O \quad (7)$$

$${}^{\cdot}CH_3 + {}^{\cdot}OH \rightarrow CH_3OH \quad (8)$$

$$CH_3OH + 2{}^{\cdot}OH \rightarrow HCOOH + H_2O + H_2 \quad (9)$$

$$2MoO_3(e^-) + 2H^+ \rightarrow H_xMoO_3 \quad (10)$$

This electron transfer facilitates the separation and transfer of photogenerated electrons and holes to the catalyst surface. Water molecules are then oxidised by photo-generated holes to generate H_2O_2 on the catalyst surface (eqn (2)). The *in situ* generated H_2O_2 could be further oxidised by the photo-generated holes to form a ˙OOH radical (eqn (3)). We consider that this is why the concentration of ˙OOH radicals over the Pd/MoO_3 catalyst were higher (Fig. 4a). Meanwhile, methane molecules are activated by photo-generated holes to form methyl radicals (eqn (4)).[41] Next, methyl hydrogen peroxide (CH_3OOH) can be generated by the reaction of methyl (˙CH_3) and hydroperoxyl radicals (˙OOH) (eqn (5)). Evidence to support the formation of CH_3OOH as an initial product comes from our previous study of methane oxidation with H_2O_2 (ref. 21) where we demonstrated that CH_3OOH was formed by the reaction of ˙CH_3 with ˙OOH. The CH_3OOH species are not stable and would be further reduced into methanol by the photo-generated electrons (eqn (6)). It is also possible that the *in situ* generated H_2O_2 can be reduced by a photo-generated electron with surface H^+ to form a hydroxyl radical (˙OH) (eqn (7)). Methanol is produced *via* the reaction of a methyl radical and a hydroxyl radical (eqn (8)). However, it has been widely reported excess ˙OH can result in over oxidation of methanol to formic acid (HCOOH) (eqn (9)).

Therefore, the primary reaction approach for methane oxidation over Pd/MoO_3 most likely proceeds *via* eqn (1)–(6). Nevertheless, the overall reaction scheme is different over the pure MoO_3 sample. Without Pd clusters, the separation of electrons and holes is difficult to achieve. Therefore, H_2O_2 reduction to ˙OH by photo-generated electrons is facile on pure MoO_3 surface (as illustrated by ESR in Fig. 4a) and as a result HCOOH is the dominate product over 12 h (Fig. S3a†).

From eqn (1)–(6), excess H^+ can be generated in the reaction cell. In parallel, we consider that these H^+ species can react with photo-generated electrons in the conduction band of MoO_3 to form $H_xMoO_3{\cdot}H_2O$ species (eqn (10)), as suggested by the XRD pattern of the used Pd/MoO_3 sample (Fig. S5†). Ideally, the H^+ species present could react to generate H_2 by photo-generated electrons, however, the conduction band potentials of MoO_3 and Pd/MoO_3 are lower than the redox potential of H^+/H_2 (−0.41 V *vs.* NHE at pH 7). Finally, the $H_xMoO_3{\cdot}H_2O$ species formed on the catalyst surface can compensate the element and charge balance for the whole reactions. These H_xMoO_3 species can be converted into MoO_3 after heat treatment in air.

4. Conclusions

Our experimental results demonstrate photo-generated holes from MoO_3 can oxidize H_2O into H_2O_2. The *in situ* generated H_2O_2 is then further decomposed into hydroxyl radicals ($^{\bullet}OH$) on the un-modified MoO_3 surface, resulting in formic acid (HCOOH) as the main product from methane oxidation. Over Pd/MoO_3, the majority of the *in situ* generated H_2O_2 can be oxidized into hydroperoxyl radicals ($^{\bullet}OOH$) by photo-generated holes, and then the dominant products from methane oxidation are CH_3OH and CH_3OOH with a combined selectivity of 98.6% within 8 h. Based on *in situ* DRIFT and photo-electrochemical measurements, the superior selectivity observed over the Pd/MoO_3 catalysts in this study for the partial methane oxidation to CH_3OH and CH_3OOH at ambient conditions is ascribed to the efficient electron transfer from MoO_3 to PdO. This can facilitate H_2O_2 generation and its decomposition into $^{\bullet}OOH$ species. These results advance the possibility to use methane as a C_1 starting material together with water and sunlight to make chemical intermediates, and to do this at ambient pressure and temperature. In this way, photocatalytic methane partial oxidation, when driven by renewable solar energy, represents a potentially 'clean' strategy for replacing energy-intensive industrial approach for methane conversion.

Author contributions

S. Sun, N. F. Dummer and G. J. Hutchings – designed the project. G. J. Hutchings – supervised the progress of the entire project. S. Sun – conducted the catalysts preparation, activity tests and sample characterizations by TEM and ESR. S. Sun and T. Bere – carried out *in situ* DRIFT measurements. S. Sun and A. J. Barnes – carried out NMR measurements. S. Sun and G. Shaw – carried out XRD and DRS measurements. M. Douthwaite, S. Pattisson and R. Lewis – contributed to other characterizations. N. Richards contributed to the analysis of XRD results. D. J. Morgan – conducted and analysed the sample by XPS. The manuscript was written through collective contributions from all authors. All authors approved the final version of the manuscript.

Conflicts of interest

There are no conflicts to declare.

Acknowledgements

This work was financially supported by the National Natural Science Foundation of China (Grant No. 22175034, 21671197) and the Shanghai Science and Technology Commission (No. 21ZR1401600). The research has also been financially supported from the European Union's Horizon 2020 research and innovation program under the Marie Skłodowska-Curie Actions (Grant Agreement No. 785794).

References

1 R. H. Crabtree, *Chem. Rev.*, 1995, **95**, 987–1007.
2 P. Schwach, X. Pan and X. Bao, *Chem. Rev.*, 2017, **117**, 8497–8520.
3 S. Wei, X. Zhu, P. Zhang, Y. Fan, Z. Sun, X. Zhao, D. Han and L. Niu, *Appl. Catal., B*, 2021, **283**, 119661.
4 Y. Song, Y. Zhao, G. Nan, W. Chen, Z. Guo, S. Li, Z. Tang, W. Wei and Y. Sun, *Appl. Catal., B*, 2020, **270**, 118888.
5 C. Oh, J. Kim, Y. J. Hwang, M. Ma and J. H. Park, *Appl. Catal., B*, 2021, **283**, 119653.
6 S. J. Blanksby and G. B. Ellison, *Acc. Chem. Res.*, 2003, **36**, 255–263.
7 M. Ravi, V. L. Sushkevich, A. J. Knorpp, M. A. Newton, D. Palagin, A. B. Pinar, M. Ranocchiari and J. A. van Bokhoven, *Nat. Catal.*, 2019, **2**, 485–494.
8 D. Zeng, Y. Qiu, M. Li, L. Ma, D. Cui, S. Zhang and R. Xiao, *Appl. Catal., B*, 2021, **281**, 119472.
9 P. Tang, Q. Zhu, Z. Wu and D. Ma, *Energy Environ. Sci.*, 2014, **7**, 2580–2591.
10 International Energy Agency (IEA), *Resources to reserves 2013*, IEA, 2013.
11 I. Dybkjær and K. Aasberg-Petersen, *Can. J. Chem. Eng.*, 2016, **94**, 607–612.
12 C. J. Jones, D. Taube, V. R. Ziatdinov, R. A. Periana, R. J. Nielsen, J. Oxgaard and W. A. Goddard III, *Angew. Chem.*, 2004, **116**, 4726–4729.
13 R. A. Periana, D. J. Taube, E. R. Evitt, D. G. Löffler, P. R. Wentrcek, G. Voss and T. Masuda, *Science*, 1993, **259**, 340–343.
14 R. A. Periana, D. J. Taube, S. Gamble, H. Taube, T. Satoh and H. Fujii, *Science*, 1998, **280**, 560–564.
15 M. Muehlhofer, T. Strassner and W. A. Herrmann, *Angew. Chem., Int. Ed.*, 2002, **41**, 1745–1747.
16 B. G. Hashiguchi, M. M. Konnick, S. M. Bischof, S. J. Gustafson, D. Devarajan, N. Gunsalus, D. H. Ess and R. A. Periana, *Science*, 2014, **343**, 1232–1237.
17 M. Ravi and J. A. van Bokhoven, *ChemCatChem*, 2018, **10**, 2383–2386.
18 T. Sheppard, C. D. Hamill, A. Goguet, D. W. Rooney and J. M. Thompson, *Chem. Commun.*, 2014, **50**, 11053–11055.
19 V. L. Sushkevich, D. Palagin, M. Ranocchiari and J. A. van Bokhoven, *Science*, 2017, **356**, 523–527.

20 X. Wang, N. M. Martin, J. Nilsson, S. Carlson, J. Gustafson, M. Skoglundh and P. A. Carlsson, *Catalysts*, 2018, **8**, 545.
21 N. Agarwal, S. J. Freakley, R. U. McVicker, S. M. Althahban, N. Dimitratos, Q. He, D. J. Morgan, R. L. Jenkins, D. J. Willock, S. H. Taylor, C. J. Kiely and G. J. Hutchings, *Science*, 2017, **358**, 223–227.
22 C. Hammond, M. M. Forde, M. H. A. Rahim, A. Thetford, Q. He, R. L. Jenkins, N. Dimitratos, J. A. Lopez-Sanchez, N. F. Dummer, D. M. Murphy, A. F. Carley, S. H. Taylor, D. J. Willock, E. E. Stangland, J. Kang, H. Hagen, C. J. Kiely and G. J. Hutchings, *Angew. Chem., Int. Ed.*, 2012, **51**, 5129–5133.
23 M. H. A. Rahim, M. M. Forde, R. L. Jenkins, C. Hammond, Q. He, N. Dimitratos, J. A. Lopez-Sanchez, A. F. Carley, S. H. Taylor, D. J. Willock, D. M. Murphy, C. J. Kiely and G. J. Hutchings, *Angew. Chem., Int. Ed.*, 2013, **52**, 1280–1284.
24 C. Williams, J. H. Carter, N. F. Dummer, Y. K. Chow, D. J. Morgan, S. Yacob, P. Serna, D. J. Willock, R. J. Meyer, S. H. Taylor and G. J. Hutchings, *ACS Catal.*, 2018, **8**, 2567–2576.
25 S. Murcia-López, K. Villa, T. Andreu and J. R. Morante, *ACS Catal.*, 2014, **4**, 3013–3019.
26 S. Murcia-López, M. C. Bacariza, K. Villa, J. M. Lopes, C. Henriques, J. R. Morante and T. Andreu, *ACS Catal.*, 2017, **7**, 2878–2885.
27 K. Villa, S. Murcia-López, T. Andreu and J. R. Morante, *Appl. Catal., B*, 2015, **163**, 150–155.
28 X. Chen, Y. Li, X. Pan, D. Cortie, X. Huang and Z. Yi, *Nat. Commun.*, 2016, **7**, 12273.
29 Y. Zhou, L. Zhang and W. Wang, *Nat. Commun.*, 2019, **10**, 506.
30 J. Xie, R. Jin, A. Li, Y. Bi, Q. Ruan, Y. Deng, Y. Zhang, S. Yao, G. Sankar, D. Ma and J. Tang, *Nat. Catal.*, 2018, **1**, 889–896.
31 M. Ravi, M. Ranocchiari and J. A. van Bokhoven, *Angew. Chem., Int. Ed.*, 2017, **56**, 16464–16483.
32 N. Fairley, V. Fernandez, M. Richard-Plouet, C. Guillot-Deudon, J. Walton, E. Smith, D. Flahaut, M. Greiner, M. Biesinger, S. Tougaard, D. Morgan and J. Baltrusaitis, *Appl. Surf. Sci. Adv.*, 2021, **5**, 100112.
33 D. O. Scanlon, G. W. Watson, D. J. Payne, G. R. Atkinson, R. G. Egdell and D. S. L. Law, *J. Phys. Chem. C*, 2010, **114**, 4636–4645.
34 X. X. Wang, J. D. Yang, H. J. Yin, R. Song and Z. Y. Tang, *Adv. Mater.*, 2013, **25**, 2728–2732.
35 E. Gracia-Espino, G. Z. Hu, A. Shchukarev and T. WÅgberg, *J. Am. Chem. Soc.*, 2014, **136**, 6626–6633.
36 X. Zhou, H. Y. Zhou, T. Y. Cheang, Z. W. Zhao, C. C. Shen, K. Liang, Y. N. Liu, Z. K. Yang, M. Imran and A. W. Xu, *J. Phys. Chem. C*, 2017, **121**, 27528–27534.
37 C. R. Henry, *Surf. Sci. Rep.*, 1998, **31**, 231–325.
38 W. Juszczyk, Z. Karpiński, I. Ratajczykowa, Z. Stanasiuk, J. Zieliński, L. L. Sheu and W. M. H. Sachtler, *J. Catal.*, 1989, **120**, 68–77.
39 J. Szanyi, W. K. Kuhn and D. W. Goodman, *J. Vac. Sci. Technol., A*, 1993, **11**, 1969–1974.
40 S. Khoobiar, *J. Phys. Chem.*, 1964, **68**, 411–412.
41 L. Chen, A. C. Cooper, G. P. Pez and H. Cheng, *J. Phys. Chem. C*, 2008, **112**, 1755–1758.
42 H. Wang, L. Zhang, K. Wang, X. Sun and W. Wang, *Appl. Catal., B*, 2019, **243**, 771–779.
43 Ș. Neatu, J. A. Maciá-Agulló, P. Concepción and H. Garcia, *J. Am. Chem. Soc.*, 2014, **136**, 15969–15976.
44 J. Baltrusaitis, J. H. Jensen and V. H. Grassian, *J. Phys. Chem. B*, 2006, **110**, 12005–12016.
45 R. Philippt and K. Fujimoto, *J. Phys. Chem.*, 1992, **96**, 9035–9038.
46 M. T. Greiner, L. Chai, M. G. Helander, W. M. Tang and Z. H. Lu, *Adv. Funct. Mater.*, 2013, **23**, 215–226.
47 H. Zhang, S. Pokhrel, Z. Ji, H. Meng, X. Wang, S. Lin, C. H. Chang, L. Li, R. Li, B. Sun, M. Wang, Y. P. Liao, R. Liu, T. Xia, L. Mädler and A. E. Nel, *J. Am. Chem. Soc.*, 2014, **136**, 6406–6420.

